AN ANALYTICAL MODEL FOR ACSR* APPROACH TO VIBRATION REDUCTION IN A HELICOPTER ROTOR/FLEXIBLE FUSELAGE SYSTEM

Thiem Chiu† and Peretz P. Friedmann‡
Mechanical and Aerospace Engineering Department
University of California, Los Angeles
Los Angeles, California USA

Abstract

This paper describes the development of a coupled rotor/flexible fuselage model which is suitable for simulating vibration reduction based on the ACSR approach. The rotor is an N_b-bladed aeroelastic model, with coupled flap-lag-torsional dynamics for each blade. Moderate blade deflections are included, together with complete coupling between rotor and fuselage dynamics. This aeroelastic response model is combined with a control algorithm based on an internal model principle. The control scheme effectively reduces vibrations to levels below 0.05g, using reasonable actuator forces. With the actuators engaged, the hub loads remain virtually unchanged and therefore this control approach has no influence on vehicle airworthiness. The magnitude of control forces and actuator power requirements are dependent on the locations where the baseline fuselage vibrations are measured; however, this sensitivity is relatively mild.

Nomenclature

a_x, a_y, a_z	Fuselage accelerations at various locations
$\mathbf{C}_c(s)$	Compensator matrix
$\mathbf{C}_d(s)$	Baseline vibration measurements, Eq. (33)
$\mathbf{D}_p(s)$	Denominator matrix of plant
EI_y, EI_z	Blade bending stiffnesses in flap and lead-lag, respectively
$\mathbf{f}_b$	Vector of blade equations
fC_{df}	Fuselage flat plate drag area
$\mathbf{F}_{d_s}$	Steady state output contribution due to disturbance
$\mathbf{f}_t$	Vector of trim equations
$\mathbf{F}_{u_s}$	Steady state output contribution due to control signal
F_x, F_y, F_z	Vibratory hub shears
$\mathbf{G}_D(s)$	Transfer matrix (Eq. 29)
$\mathbf{G}^D(s)$	Transfer matrix (Eq. 43)
GJ	Blade torsional stiffness
$\mathbf{G}_u(s)$	Transfer matrix (Eq. 28)
$\mathbf{G}^u(s)$	Transfer matrix (Eq. 44)
$\mathbf{G}_{y_d}(j\omega_d)$	Disturbance transfer matrix at rotor passage frequency
$\mathbf{G}_{y_u}(j\omega_d)$	Control transfer matrix at rotor passage frequency
$\mathbf{H}_D(s)$	Constant matrix (Eq. 45)
$\mathbf{H}_u(s)$	Constant matrix (Eq. 46)
M	Consistent mass matrix of non-structural mass element
m_b	Blade mass per unit length
M_x, M_y, M_z	Vibratory hub moments
N_b	Number of blades
$\mathbf{N}_p$	Numerator matrix of plant
q	Number of modes retained in modal truncation
$\mathbf{q}_b$	Vector of blade degrees of freedom
$q_{b_o}, q_{b_{nc}}, q_{b_{ns}}$	Harmonic components of blade degrees of freedom
$\mathbf{q}_e$	Vector of fuselage elastic degrees of freedom
$q_{e_o}, q_{e_{nc}}, q_{e_{ns}}$	Harmonic components of fuselage elastic response
$\mathbf{q}_f$	Vector of fuselage rigid body degrees of freedom
$q_{f_o}, q_{f_{nc}}, q_{f_{ns}}$	Harmonic components of fuselage rigid body response
$q_{\phi_i}, q_{v_i}, q_{w_i}$	Generalized coordinates of blade torsional, lag and flap degrees of freedom
R	Rotor radius
R_x, R_y, R_z	Fuselage rigid body translational degrees of freedom
u, v, w	Blade displacement components
$\mathbf{U}(t)$	Actuator control signal vector
$\mathbf{U}_o$	Control amplitudes
x	Blade spanwise coordinate
$\mathbf{X}(t)$	Fuselage elastic states (modal domain)
$X_d(t)$	Disturbance state
X_{d_o}	Initial conditions for disturbance state
$\mathbf{X}_o$	Initial conditions for fuselage elastic states

Greek Symbols

α_R	Rotor angle of attack
ε	Non-dimensional parameter representing order of magnitude of typical blade slope

*Active Control of Structural Response
†Postdoctoral Scholar
‡Professor

θ_o	Collective pitch
θ_{1c}, θ_{1s}	Cyclic pitch components
$\theta_x, \theta_y, \theta_z$	Fuselage roll, pitch and yaw degrees of freedom
λ	Inflow ratio
Λ_q	Matrix containing fuselage natural frequencies
μ	Advance ratio
Ω	Angular speed of rotor
ω_d	Disturbance frequency
ψ	Blade azimuth angle, nondimensional time($= \Omega$ t)
$\phi(s)$	Unstable poles of disturbance loads in Laplace domain
ϕ_s	Rotor roll angle
$\Phi_{w_i}, \Phi_{v_i}, \Phi_{\phi_i}$	Rotating mode shapes for blade flap, lag and torsional response
$\omega_{F_1}, \omega_{F_2}, \omega_{F_3}$	Rotating blade flap frequencies
$\omega_{L_1}, \omega_{L_2}$	Rotating blade lag frequencies
$\omega_{T_1}, \omega_{T_2}$	Rotating blade torsional frequencies
ρ	Mass density of beam
ρ_A	Air density
ρ_M	Equivalent density function

Special Symbols

$(\bullet)_{,x}$	Derivative of $(\bullet)$ with respect to spanwise coordinate x
$(\dot{\bullet})$	Derivative of $(\bullet)$ with respect to time

Introduction and Problem Statement

The control of vibrations in helicopters, which consists of reducing vibration levels below specified limits, is one of the key problems facing the rotorcraft designer. The increasing demands on flight envelope expansion, such as nap of earth flying, high speed, high g maneuvers, coupled with the need to improve system reliablity and reduce maintenance costs has resulted in more stringent vibration specifications. The adoption of ADS-27 [1,2] by the U.S. Army illustrates the increased emphasis placed on the developpment of rotorcraft with drastically reduced vibration levels. There has been a steady decrease in rotorcraft vibration levels over the years. The adoption of stringent vibration requirements, for the next generation of helicopters, implies reduction of vibration levels below 0.05 g or even 0.02 g. Therefore, a substantial body of research and development effort has been directed toward vibration prediction and reduction methodologies in helicopters [3-5]. A detailed summary of the NASA/Army contributions to rotorcraft vibration technology has been presented in an excellent paper [5].

It is well known that the principal contributors to vibration levels in the helicopter fuselage are the main and tail rotor systems, as well as the aerodynamic interaction between the rotor and the fuselage [3, 4]. The central need for vibration reduction in helicopter design has led to the development of two fundamentally different approaches to vibration reduction and alleviation. The first approach is passive and it utilizes vibration absorbers and vibration isolation devices [3-5], another passive approach is the careful structural dynamic design using structural optimization aimed at minimizing vibration in forward flight [6]. The second approach is active, and it is based on using active control for vibration reduction. These approaches have been described and reviewed with considerable detail in a recent paper [7]. Among the more recent approaches to active control of vibration, two approaches seem to have considerable promise. One approach is the actively controlled flap (ACF), located at the outboard portion of the blade, which has been shown to achieve vibration levels comparable to higher harmonic control (HHC), while consuming much less power [7]. Another new approach to active control of fuselage vibration is active control of structural response (ACSR) which was initially developed by Westland [8]. Recently, a modified variant of the ACSR approach, known as active vibration reduction (AVR), has been also explored and flight tested [9, 10]. In this approach, the gearbox is being oscillated instead of an ACSR platform.

The ACSR scheme is based on the idea that in a linear system one can superimpose two independent response quantities such that the total response is zero. A schematic representation of the ACSR system is shown in Figs. 1 and 2. Figure 1 depicts the flexible fuselage model with the ACSR platform which is assumed to be a rigid platelike structure. The four actuators, depicted by the four heavy vertical lines are located at the corners of the platform and these introduce oscillatory forces used for vibration reduction. The bottom and top of these actuators are designated by $p_1, \ldots, p_8$, respectively. A schematic diagram of the ACSR control system is depicted in Fig. 2. When applying this scheme to the helicopter vibration reduction problem, the fuselage, at selected locations, is excited by controlled forcing inputs, such that the combined response of the fuselage, due to rotor loads and the applied excitations, is minimized. Ground and flight test performed on a Westland 30 four-bladed hingeless helicopter were described in Ref. 11. Preliminary experimental tests with the ACSR system have produced very promising results for vibration control in helicopters [11,12]. The major advantages of this new scheme are: (a) ability to minimize vibrations at specific fuselage locations; (b) low power requirements; and (c) simplicity and minimal impact on air worthiness, because vibration control is implemented entirely in the nonrotating system.

Despite the initial success with the ACSR system, recent flight tests [13] have indicated a somewhat limited vibration reduction capability, when compared to the earlier tests. This emphasizes the importance of an analytical simulation capability that can provide fundamental understanding needed for the successful implementation of the ACSR approach. A refined coupled rotor/flexible fuselage aeroelastic response analysis suitable for the modeling of vibration reduction based upon the ACSR approach has been recently developed by the authors [14-16], and it has been used by the authors in a number of vibration reduction studies.

The current paper has several objectives: (a) describe a coupled rotor/flexible fuselage aeroelastic response model, including the actuators required for the simulation of an ACSR system on a typical helicopter; (b) present a recently completed vibration reduction study employing a disturbance rejection scheme based on an internal model principle (IMP) for the controller; and (c) determine the sensitivity of the actuator forces needed for vibration suppression to changes in the location of the sensors, which measure the vibration levels in the fuselage.

It is important to note that relatively few coupled rotor/flexible fuselage aeroelastic response models capable of modeling the vibration levels present in such a complicated structural dynamic system exist. Most coupled rotor/fuselage models available, combine a rotor with a number of flexible blades with a fuselage represented by *rigid body degrees of freedom*, and such models are usually aimed at studying the aeromechanical stability behavior in forward flight [17,18]. A few coupled rotor/flexible fuselage models exist. Typical of these is Ref. 19, which combines a flexible rotor with a flexible fuselage. The fuselage model was relatively simple, since it consisted of a flexible beam with bending flexibility in two mutually perpendicular planes combined with twist about the beam axis. Reference 19 did not account for the presence of non-structural masses in the modeling of the fuselage. Other studies [20, 21] have represented the coupled rotor/flexible fuselage model by a one dimensional beam, where the beam itself is modeled by beam type finite elements. Unfortunately, none of these models are capable of modeling the refined local vibration level modeling needed for simulating the ACSR system. Thus, the current paper attempts to remedy this situation by developing an analytical simulation capability suitable for vibration reduction studies using ACSR; and it also makes a substantial contribution toward improved coupled rotor/flexible fuselage aeroelastic response modeling.

Mathematical Formulation

The coupled rotor/flexible fuselage model, developed in this study, is capable of representing flexible hingeless rotor combined with a flexible fuselage, a platform for the ACSR system and four high frequency force actuators located at the corners of the platform. The model is capable of representing both four (as shown in Fig. 1) and five bladed rotors. For clarity, the description of the model is separated in its components: the rotor, the fuselage with an ACSR platform and actuators. For active vibration reduction studies the aeroelastic response model is combined with a controller based on an *internal model principle* (IMP) and sensors distributed at specific locations in the fuselage.

The Rotor Model

The current study is based upon a flexible hingeless blade model with coupled flap-lag-torsional dynamics, and the geometrically nonlinear terms due to moderate deflections. The nonlinear partial differential equations describing the blade dynamics of an isolated rotor blade are given by Eqs. (5) - (7) of Ref. 22. These equations were derived for the case of an isolated blade. However, the structural operator in these equations is not affected by fuselage dynamics, and thus it is suitable for the present study.

The distributed aerodynamic, gravitational and inertial load vectors per unit length are symbolically derived to obtain the total distributed force and moment vectors acting on the blade. These loads, which include the contribution of the fuselage motion to the inertial and aerodynamic blade loads, are derived using a symbolic manipulation program MACSYMA [23].

The aerodynamic loads are obtained from Greenberg's quasi-steady aerodynamic theory [24]; whereas the inertial loads are based on D'Alembert's principle. The reverse flow region on the blade is accounted for by changing the direction of the drag and setting the lift and moment equal to zero. Stall and compressibility effects are neglected, and constant uniform inflow is assumed. The inextensional assumption for the axial deformation of the blade; commonly used in rotary-wing aeroelasticity [19, 22, 25], is employed to express the blade axial deformation in terms of it bending deformations.

The inertial and aerodynamic loads are derived explicitly using an ordering scheme [17-21] which allows one to have expressions of manageable size when fuselage dynamics are included. Such ordering schemes have been also used in other similar studies involving coupled rotor/flexible fuselage dynamics [20,21]. The ordering scheme is based on the assumption that:

$$1 + O(\varepsilon^2) \cong 1 \tag{1}$$

where ε is a small dimensionless parameter on the order of a typical blade slope. Equation (1) implies that terms of the order ε^2 are negligible compared to unity.

The Fuselage Model

The elastic fuselage is represented by a complete three dimensional structural model. A collection of elements (i.e. element library) is used to generate the structural dynamic model of the fuselage. The elements available are: beam, truss, non-structural mass, and a plate element. The non-structural masses of the helicopter such as: fuel tanks, engine, transmission, gearing, and payload, etc., are also modeled using consistently derived finite element model [26]. The non-structural mass element is capable of three translational displacements and three rotational degrees of freedom at each node. The consistent mass matrix for the non-structural mass element is obtained from the following equation:

$$\mathbf{M} = \int_0^l \int_A \mathbf{N}^T \mathbf{N} \rho_M \, dA dx \tag{2}$$

The shape function matrix is represented by the matrix $\mathbf{N}$ and the vector ρ_M denotes the equivalent density functions. The non-structural mass per unit length is modeled by an equivalent density function defined over the length of the beam element l such that the product of ρ_M and the beam cross sectional area integrated over it length contributes an amount of mass equal to the non-structural mass. Separate density functions are considered for axial, torsion, and bending. Analytical expressions for these equivalent density functions can be found in Ref. 26.

A realistic structural dynamic model for the helicopter fuselage requires the representation of the concentrated masses as shown in Fig. 1. Numerical results, for mode shapes and frequencies, indicate that if concentrated masses are not properly accounted for in the fuselage model, the modal characteristics of a real helicopter fuselage can not be captured [27].

The ACSR Platform and Actuators

The coupled rotor/flexible fuselage model has a provision for incorporating an ACSR platform. This platform consists of a rigid rectangular plate inserted between the rotor and the flexible fuselage. At the four corners of the platform, the model can accomodate high frequency force actuators, which produce very small displacements, but considerable force. These are illustrated by the heavy vertical lines shown in Fig. 1 and the end points of the actuators correspond to points $p_1, \ldots, p_8$ in Fig. 1, respectively. Provision is made for measuring accelerations at a discrete number of fuselage locations. For the current study, the sensors are placed at the pilot seat, mid-cabin and rear cabin locations, and measure the vibration levels at these locations. The complete mathematical model describing the active controller for these actuators together with results illustrating their potential for vibration reduction will be presented later in this paper.

Description of Solution Procedure

The first step in the solution of the problem is to eliminate the spatial dependence in the blade equations of motion. The system of coupled partial differential equations of motion is transformed to a system of ordinary nonlinear differential equations by using Galerkin's method to eliminate the spatial variable. In this process, two torsional, two lead-lag, and three flap, uncoupled, free vibration modes of a rotating cantilevered blade are used. For the coupled rotor/fuselage system in steady state forward flight, only the periodic nonlinear steady state response is required. In this study, the trim and response solutions are obtained in a single pass by simultaneously satisfying the trim equilibrium and the vibratory response of the helicopter for all the rotor and fuselage degrees of freedom [19]. The coupled solution is obtained using the harmonic balance technique. In the harmonic balance method, one replaces a system of ordinary differential equations of motion in the time domain by a system of algebraic equations with constant coefficients in the frequency domain. This solution yields the steady state response. The transformation to the frequency domain is accomplished by a Fourier series expansion of various degrees of freedom representing the coupled dynamics of the rotor/flexible fuselage dynamic system. To illustrate this procedure, the equations of motion for the coupled rotor/fuselage system are symbolically represented as:

$$\mathbf{f}_b(q, \dot{q}, \ddot{q}, q_t; \psi) = 0 \tag{3}$$

$$\mathbf{f}_f(q, \dot{q}, \ddot{q}, q_t; \psi) = 0 \tag{4}$$

$$\mathbf{f}_e(q, \dot{q}, \ddot{q}, q_t; \psi) = 0 \tag{5}$$

$$\mathbf{f}_t(q, \dot{q}, \ddot{q}, q_t; \psi) = 0 \tag{6}$$

Equation (3) represents the coupled blade flap-lag-torsional equations of motion. The vectors $\mathbf{f}_f$, $\mathbf{f}_e$, and $\mathbf{f}_t$ correspond to the fuselage rigid body equations of motion, the fuselage elastic motion, expressed in modal domain, and the trim equations, respectively. The vector $\mathbf{q}_t$ represents the trim solution which consists of the quantities $\lambda, \theta_o, \theta_{1c}, \theta_{1s}, \alpha_R$, and ϕ_s. The response vector $\mathbf{q}$ consists of the blade degrees of freedom, the fuselage rigid body degrees of freedom, and the fuselage elastic generalized displacements. These quantities are represented by the solution vector $\mathbf{q}$,

$$\mathbf{q} = \left\{ \begin{array}{c} \mathbf{q}_b \\ \mathbf{q}_f \\ \mathbf{q}_e \end{array} \right\} \tag{7}$$

The vector $\mathbf{q}_b$ represents the blade response in the flap, lag and torsion, i.e.,

$$\mathbf{q}_b = \left\{ \begin{array}{c} w \\ v \\ \phi \end{array} \right\} \tag{8}$$

The blade response is approximated by two rotating modes for torsion and lag response, and three rotating modes for flap, i.e.,

$$\phi = \sum_{i=1}^{2} \Phi_{\phi_i}(x) q_{\phi_i}(t) \qquad (9)$$

$$v = \sum_{i=1}^{2} \Phi_{v_i}(x) q_{v_i}(t)$$

$$w = \sum_{i=1}^{3} \Phi_{w_i}(x) q_{w_i}(t)$$

The vector $\mathbf{q}_f$ represents the fuselage's rigid body translational and rotational responses, i.e.,

$$\mathbf{q}_f = \left\{ \begin{array}{c} R_x \\ R_y \\ R_z \\ \theta_x \\ \theta_y \\ \theta_z \end{array} \right\} \qquad (10)$$

The vector $\mathbf{q}_e$ represents the elastic deformations of the fuselage in the modal domain, i.e.,

$$\mathbf{q}_e = \left\{ \begin{array}{c} \xi_1 \\ \vdots \\ \xi_n \end{array} \right\} \qquad (11)$$

where n represents the truncated number of flexible fuselage modes retained in the model.

Since the dominant components of the rotor loads transmitted to the fuselage through the hub are integer multiples of the rotor passage frequency $n_i N_b$, the combined response of the fuselage, consisting of a combination of rigid body and elastic degrees of freedom, will contain primarily integer multiples of N_b per rev harmonics. In steady forward flight, a periodic solution in the form of Fourier series is assumed for the blade and fuselage degrees of freedom [19]; which can be written as:

$$\mathbf{q}_b = \mathbf{q}_{b_o} + \sum_{n=1}^{N_H} \{ \mathbf{q}_{b_{nc}} cos(n\psi) + \mathbf{q}_{b_{ns}} sin(n\psi) \} \qquad (12)$$

$$\mathbf{q}_f = \mathbf{q}_{f_o} + \sum_{n=1}^{N_f} \{ \mathbf{q}_{f_{nc}} cos(nN_b\psi) + \mathbf{q}_{f_{ns}} sin(nN_b\psi) \} \qquad (13)$$

$$\mathbf{q}_e = \mathbf{q}_{e_o} + \sum_{n=1}^{N_e} \{ \mathbf{q}_{e_{nc}} cos(nN_b\psi) + \mathbf{q}_{e_{ns}} sin(nN_b\psi) \} \qquad (14)$$

where N_H, N_f, and N_e represent truncated harmonics for the blade, fuselage rigid body, and fuselage elastic degrees of freedom, respectively.

The equations of motion represented by Eqs. (3) to (6) can be expressed explicitly in terms of the Fourier series expansion coefficients by subsituting Eqs. (12) to (14) into Eqs. (3) to (6) and applying the harmonic balance technique to yield a system of nonlinear coupled algebraic equations. The resulting equations of motion, for the expansion coefficients, can be symbolically represented by:

$$\mathbf{f}_b = \mathbf{f}_{b_o} + \sum_{n=1}^{N_H} \{ \mathbf{f}_{b_{nc}} cos(n\psi) + \mathbf{f}_{b_{ns}} sin(n\psi) \} \qquad (15)$$

where

$$\mathbf{f}_{b_o} = \frac{1}{2\pi} \int_0^{2\pi} \mathbf{f}_b(q, \dot{q}, \ddot{q}, q_t; \psi)\, d\psi \qquad (16)$$

$$\mathbf{f}_{b_{nc}} = \frac{1}{\pi} \int_0^{2\pi} \mathbf{f}_b(q, \dot{q}, \ddot{q}, q_t; \psi) cos(n\psi)\, d\psi$$

$$\mathbf{f}_{b_{ns}} = \frac{1}{\pi} \int_0^{2\pi} \mathbf{f}_b(q, \dot{q}, \ddot{q}, q_t; \psi) sin(n\psi)\, d\psi$$

The equation $\mathbf{f}_{b_o}$ represents the constant parts of the blade flap-lag-torsional equation of motion; and the vectors $\mathbf{f}_{b_{nc}}$ and $\mathbf{f}_{b_{ns}}$ denote the cosine and sine parts of the blade equations, respectively.

In order to properly enforce the coupling between the rotor and the fuselage, the rotor inertial, aerodynamic, gravitational, and damping loads are first transferred to the hub, then transformed to the non-rotating reference frame before they are combined with the corresponding fuselage loads. The fuselage rigid body motion is symbolically represented by Eq. (4). To clarify the coupling between the fuselage rigid body, and all other degrees of freedom, the rigid body equations of motion are symbolically rewritten as:

$$\mathbf{P}_b^I + \mathbf{P}_b^A + \mathbf{P}_b^G + \mathbf{P}_b^D + \mathbf{P}_{fus} = \mathbf{0} \qquad (17)$$

$$\mathbf{Q}_b^I + \mathbf{Q}_b^A + \mathbf{Q}_b^G + \mathbf{Q}_b^D + \mathbf{Q}_{fus} = \mathbf{0} \qquad (18)$$

The vectors $\mathbf{P}_b^I$,$\mathbf{P}_b^A$,$\mathbf{P}_b^G$ and $\mathbf{P}_b^D$ represent the blade inertial, aerodynamic, gravitational, and damping force vectors, respectively, whereas the vector $\mathbf{P}_{fus}$ denotes the summation of all the fuselage force contributions. In a similar manner, the components of the moment vector $\mathbf{Q}_b^I$,$\mathbf{Q}_b^A$,$\mathbf{Q}_b^G$, $\mathbf{Q}_b^D$ and $\mathbf{Q}_{fus}$ represent the appropriate moment contributions. Equations (17) and (18) represent force and moment equilibrium that is enforced at the hub. This coupling procedure accounts for all the contributions in an exact manner; and it does not require the approximations described in Ref. 28.

The fuselage rigid body equations of motion are also expanded in Fourier series, i.e.,

$$\begin{aligned} \mathbf{f}_f &= \mathbf{f}_{f_o} + \sum_{n=1}^{N_f} \{\mathbf{f}_{f_{nc}} cos(nN_b\psi) + \\ &\quad \mathbf{f}_{f_{ns}} sin(nN_b\psi)\} \end{aligned} \tag{19}$$

where

$$\mathbf{f}_{f_o} = \frac{1}{2\pi}\int_0^{2\pi} \mathbf{f}_f(q,\dot{q},\ddot{q},q_t;\psi)\, d\psi \tag{20}$$

$$\mathbf{f}_{f_{nc}} = \frac{1}{\pi}\int_0^{2\pi} \mathbf{f}_f(q,\dot{q},\ddot{q},q_t;\psi) cos(nN_b\psi)\, d\psi$$

$$\mathbf{f}_{f_{ns}} = \frac{1}{\pi}\int_0^{2\pi} \mathbf{f}_f(q,\dot{q},\ddot{q},q_t;\psi) sin(nN_b\psi)\, d\psi$$

The vectors $\mathbf{f}_{f_o}$, $\mathbf{f}_{f_{nc}}$ and $\mathbf{f}_{f_{ns}}$ represent the constant parts, cosine and sine parts of the coupled rotor/fuselage rigid body equations of motion, respectively.

The three dimensional fuselage model is represented by a system of second order ordinary differential equations with constant coefficients. The considerable number of flexible degrees of freedom present in the finite element model of the fuselage, are reduced by using a normal mode transformation based upon a truncated number of free vibration mode shapes. The fuselage elastic equations are also expressed in terms of the Fourier series coefficients, i.e.,

$$\begin{aligned} \mathbf{f}_e &= \mathbf{f}_{e_o} + \sum_{n=1}^{N_e} \{\mathbf{f}_{e_{nc}} cos(nN_b\psi) + \\ &\quad \mathbf{f}_{e_{ns}} sin(nN_b\psi)\} \end{aligned} \tag{21}$$

where

$$\mathbf{f}_{e_o} = \frac{1}{2\pi}\int_0^{2\pi} \mathbf{f}_e(q,\dot{q},\ddot{q},q_t;\psi)\, d\psi \tag{22}$$

$$\mathbf{f}_{e_{nc}} = \frac{1}{\pi}\int_0^{2\pi} \mathbf{f}_e(q,\dot{q},\ddot{q},q_t;\psi) cos(nN_b\psi)\, d\psi$$

$$\mathbf{f}_{e_{ns}} = \frac{1}{\pi}\int_0^{2\pi} \mathbf{f}_e(q,\dot{q},\ddot{q},q_t;\psi) sin(nN_b\psi)\, d\psi$$

The vectors $\mathbf{f}_{e_o}$, $\mathbf{f}_{e_{nc}}$ and $\mathbf{f}_{e_{ns}}$ represent the constant parts, cosine and sine parts of the fuselage elastic equations of motion in the modal domain, respectively.

The trim equations, fuselage rigid body equations, and rotor blade equations are combined and solved simultaneously. The propulsive trim procedure, based on invoking force and moment equilibrium is used to generate the solution vector. The IMSL subroutine, DNEQNF, which is suitable for the solution of a system of nonlinear algebraic equations is used [29].

After the trim and response solution has been found, the rotor vibratory hub loads are determined. The loads at the root of the k^{th} blade are obtained in the rotating frame by integrating the distributed loads along the span of the blade. These rotating loads at the blade root are transformed to the hub fixed nonrotating reference frame. Summation of the contribution from the various blades yields the total vibratory hub loads. For an N_b-bladed rotor, the vibratory hub loads are primarily N_b/rev. In this study, the hub shear and moment amplitudes are defined as follow:

$$|P_i| = \sqrt{P_{i_{N_b C}}^2 + P_{i_{N_b S}}^2} \tag{23}$$

$$|M_i| = \sqrt{M_{i_{N_b C}}^2 + M_{i_{N_b S}}^2}$$

where

$$\begin{aligned} P_{H_i} &= P_{i_o} + P_{i_{N_b C}} cos(N_b\psi) + \\ &\quad P_{i_{N_b S}} sin(N_b\psi) \end{aligned} \tag{24}$$

$$\begin{aligned} M_{H_i} &= M_{i_o} + M_{i_{N_b C}} cos(N_b\psi) + \\ &\quad M_{i_{N_b S}} sin(N_b\psi) \end{aligned}$$

where the index i denotes the Cartesian coordinates x,y and z, respectively.

The constant parts of the hub shear and moment components in the nonrotating reference frame are denoted by P_{i_o} and M_{i_o}. Similarly, the N_b/rev cosine and sine hub shear and moment components are denoted by $P_{i_{N_b C}}$, $P_{i_{N_b S}}$ and $M_{i_{N_b C}}$, $M_{i_{N_b S}}$, respectively.

Disturbance Rejection Scheme Based on an Internal Model Principle

A helicopter in steady state trimmed level forward flight experiences vibratory loads which are generated by the rotor and transmitted to the fuselage. In the framework of the control scheme implemented in this study, these vibratory loads are considered to be the disturbance loads. To counteract the disturbances, the servo actuators at the four corner of the ACSR platform, shown in Fig. 1, introduce vibratory forces, at the rotor disturbance frequency ($\omega_d = N_b\Omega$), to the rotor/gearing unit supported by the ACSR platform, so as to prevent the disturbances (or vibratory loads) from propagating into the fuselage. For the helicopter vibration problem, the frequency of the vibratory disturbances, and their points of application are usually known. This information facilitates the construction of a disturbance rejection scheme for this particular case. The ACSR scheme is based on the concept that in a linear system one can superimpose two independent response quantities in such a manner that the total response is zero. When applying this scheme to the helicopter vibration reduction problem, the fuselage, at selected locations, is excited by controlled forcing inputs, such that the combined response of the fuselage, due to rotor loads and the applied excitations, is minimized.

A mathematical model for the ACSR system including sensors and four actuators has been described earlier in this paper. In this section, a controller based on a disturbance rejection algorithm is combined with the aeroelastic model of the coupled rotor/flexible fuselage system [15,16]. The control signals are fed to the force generators (i.e., servo actuators) that generate the oscillatory loads, which are superimposed on the rotor disturbances so that the combined vibratory loads governed by the compensating control signals and the disturbances, cancel each other at the appropriate fuselage locations.

The control approach used here represents a generalization of a very simple model used in an early study [30] which explored vibration suppression in a two degree of freedom spring mass damper system, which was assumed to roughly resemble a coupled rotor/fuselage system. In this simple model, both the rotor and the fuselage were represented by lumped masses [30].

In this section, an approach denoted the IMP is implemented to improve the robustness of the control algorithm described in our earlier studies [15,16], by reducing the sensitivity of the feedback system, shown in Fig. 3, to the parameter variations of the plant [31]. The internal model is used to achieve disturbance rejection by cancelling either the unstable modes or modes on the imaginary axis, of the disturbance signals, by duplicating these modes inside the loop [31]. The theoretical basis of IMP is described in Ref. 31. The control force vector, required for its implementation, is obtained from the procedure described below. This represents an improvement on a simpler controller used in our earlier work [16].

The placement of the internal model for disturbance rejection is depicted in the block diagram in Fig. 3. The plant is given by the transfer matrix $\mathbf{G}_u(s) = \mathbf{D}_p^{-1}(s)\mathbf{N}_p(s)$, the compensator is given by the matrix $\mathbf{C}_c(s) = \mathbf{D}_c^{-1}(s)\mathbf{N}_c(s)$, and the internal model is represented by the matrix $\mathbf{D}_I^{-1}(s)$. The reference signal, r, is assumed to be zero in this study. The design procedure involves two steps: the introduction of the internal model, $\mathbf{D}_I^{-1}(s)$, inside the loop, and the use of compensator $\mathbf{C}_c(s)$ to stabilize the unity feedback system as illustrated in Fig. 3. The introduction of the disturbance dynamic model inside the loop is often referred to as the "internal model principle" [31]. If the affect of the disturbance $\mathbf{D}(s)$ at the output of the feedback system y, as shown in Fig. 3, is required to approach zero as $t \to \infty$, with the reference signal $r = 0$, then the problem is called disturbance rejection [31].

In terms of the parameters of the helicopter model, the output $\mathbf{y}(s)$ in Fig. 3, which represents the total forces transmitted across the actuators, is given by:

$$\begin{aligned} \mathbf{y}(s) &= \left\{\mathbf{C}(s\mathbf{I}-\mathbf{A})^{-1}\mathbf{B}+\mathbf{I}\right\}\mathbf{U}(s) + \\ &\quad \left\{\mathbf{C}(s\mathbf{I}-\mathbf{A})^{-1}\mathbf{E}\right\}\mathbf{D}(s) \\ &= \mathbf{G}_u(s)\mathbf{U}(s)+\mathbf{G}_D(s)\mathbf{D}(s) \end{aligned} \tag{25}$$

where the matrices $\mathbf{A}, \mathbf{B}, \mathbf{C}$ and $\mathbf{E}$ are coefficients of a state space equation representing the fuselage dynamics and the total forces transmitted across the actuators, i.e.,

$$\dot{\chi}(t) = \mathbf{A}\chi(t) + \mathbf{B}\mathbf{U}(t) + \mathbf{E}\mathbf{D}(t) \tag{26}$$

$$\mathbf{y}(t) = \mathbf{C}\chi(t) + \mathbf{U}(t) \tag{27}$$

the vector $\chi(t)$ represents the fuselage elastic degrees of freedom and the transfer matrices $\mathbf{G}_u(s)$ and $\mathbf{G}_D(s)$ are defined by:

$$\mathbf{G}_u(s) = \mathbf{C}(s\mathbf{I}-\mathbf{A})^{-1}\mathbf{B}+\mathbf{I} \tag{28}$$

and

$$\mathbf{G}_D(s) = \mathbf{C}(s\mathbf{I}-\mathbf{A})^{-1}\mathbf{E} \tag{29}$$

In an alternative form, the matrices $\mathbf{G}_u(s)$ and $\mathbf{G}_D(s)$ are represented by:

$$\mathbf{G}_u(s) = \mathbf{D}_p^{-1}(s)\mathbf{N}_p(s) \tag{30}$$

and

$$\mathbf{G}_D(s) = \mathbf{D}_p^{-1}(s)\mathbf{N}_D(s) \tag{31}$$

where the matrices $\mathbf{D}_p(s)$ and $\mathbf{N}_p(s)$ are coprime, i.e., they have no nontrivial common factors. The same statement applies to the matrices $\mathbf{D}_p(s)$ and $\mathbf{N}_D(s)$.

The disturbance signal $\mathbf{D}(s)$ in the Laplace domain is defined by:

$$\mathbf{D}(s) = \mathbf{D}_{dist}^{-1}(s)\mathbf{N}_{dist}(s) \tag{32}$$

The disturbance loads can be expressed in terms of the disturbance state in the time domain:

$$\mathbf{D}(t) = \mathbf{C}_d\chi_d(t) \tag{33}$$

and the disturbance state $\chi_d(t)$ satisfies a first order linear differential equation [16], i.e.,

$$\dot{\chi}_d(t) = A_d\chi_d(t) \tag{34}$$

where the scalar A_d is the N_b/rev rotor disturbance frequency.

To incorporate the IMP, define $\phi(s)$ as the least common denominator of the unstable poles of $\mathbf{D}(s)$, i.e., all roots of $\phi(s)$ have zero or positive real parts.

The internal model matrix $\mathbf{D}_I^{-1}(s)$ in Fig. 3 is defined by [31]:

$$\mathbf{D}_I^{-1}(s) = \phi(s)^{-1}\mathbf{I}_Q \quad (35)$$

where the identity matrix $\mathbf{I}_Q$ has dimension Q; for the current case, Q = 6.

From Fig. 3, the contributions to the output $\mathbf{y}(s)$ by the disturbance and control signals for the case of a unity feedback loop are given by:

$$\mathbf{y}(s) = \mathbf{y}_d(s) + \mathbf{y}_u(s) \quad (36)$$

where

$$\begin{aligned}\mathbf{y}_d(s) &= \mathbf{D}_p^{-1}(s)\left[\mathbf{I} + \mathbf{N}_p(s)\mathbf{N}_c(s)\mathbf{D}_c^{-1}(s)\right. \\ &\left. *\mathbf{D}_I^{-1}(s)\mathbf{D}_p^{-1}(s)\right]^{-1}\mathbf{N}_D(s)\mathbf{D}(s) \quad (37)\end{aligned}$$

$$\begin{aligned}\mathbf{y}_u(s) &= \mathbf{D}_p^{-1}(s)\left[\mathbf{I} + \mathbf{N}_p(s)\mathbf{N}_c(s)\mathbf{D}_c^{-1}(s)\right. \\ &\left. *\mathbf{D}_I^{-1}(s)\mathbf{D}_p^{-1}(s)\right]^{-1}\mathbf{N}_p(s)\mathbf{U}(s) \quad (38)\end{aligned}$$

Substituting Eqs. (32) and (35) into Eqs. (37) and (38), the outputs due to disturbance and control signals $\mathbf{y}_d(s)$ and $\mathbf{y}_u(s)$ can be rewritten as:

$$\begin{aligned}\mathbf{y}_d(s) &= \phi(s)\mathbf{D}_c(s)\left[\phi(s)\mathbf{D}_p(s)\mathbf{D}_c(s) + \mathbf{N}_p(s)\right. \\ &\left. *\mathbf{N}_c(s)\right]^{-1}\mathbf{N}_D(s)\mathbf{D}_{dist}^{-1}(s)\mathbf{N}_{dist}(s) \quad (39)\end{aligned}$$

$$\begin{aligned}\mathbf{y}_u(s) &= \phi(s)\mathbf{D}_c(s)\left[\phi(s)\mathbf{D}_p(s)\mathbf{D}_c(s) + \mathbf{N}_p(s)\right. \\ &\left. *\mathbf{N}_c(s)\right]^{-1}\mathbf{N}_p(s)\mathbf{D}_{dist}^{-1}(s)\mathbf{N}_{dist}(s) \quad (40)\end{aligned}$$

For the present case, the matrices $\phi(s)\mathbf{D}_p(s)$ and $\mathbf{N}_p(s)$ are coprime and therefore the roots of the determinant of

$$\begin{aligned}\mathbf{D}_f(s) &= \phi(s)\mathbf{D}_p(s)\mathbf{D}_c(s) + \\ &\mathbf{N}_p(s)\mathbf{N}_c(s) \quad (41)\end{aligned}$$

can be arbitrarily placed with the proper choice of the compensator $\mathbf{D}_c(s)$ and $\mathbf{N}_c(s)$ matrices, by placing these roots in the open left-half plane. Hence, the output $\mathbf{y}(s)$ (Eq. 36) will approach zero as $t \to \infty$, for a steady state process.

The control vector $\mathbf{U}(s)$, needed for vibration suppression, can be obtained by the following procedure. First, express Eq. (36) as follows:

$$\mathbf{y}(s) = \mathbf{G}^D(s)\mathbf{D}(s) + \mathbf{G}^u(s)\mathbf{U}(s) \quad (42)$$

Using Eqs. (39) and (40), the matrices $\mathbf{G}^D(s)$ and $\mathbf{G}^u(s)$ are determined as:

$$\begin{aligned}\mathbf{G}^D(s) &= \phi(s)\mathbf{D}_c(s)\left[\phi(s)\mathbf{D}_p(s)\mathbf{D}_c(s) +\right. \\ &\left. *\mathbf{N}_p(s)\mathbf{N}_c(s)\right]^{-1}\mathbf{N}_D(s) \quad (43)\end{aligned}$$

$$\begin{aligned}\mathbf{G}^u(s) &= \phi(s)\mathbf{D}_c(s)\left[\phi(s)\mathbf{D}_p(s)\mathbf{D}_c(s) +\right. \\ &\left. *\mathbf{N}_p(s)\mathbf{N}_c(s)\right]^{-1}\mathbf{N}_p(s) \quad (44)\end{aligned}$$

The transfer matrices $\mathbf{G}^D(s)$ and $\mathbf{G}^u(s)$ can be expanded as follows [31]:

$$\mathbf{G}^D(s) = \sum_{i=0}^{m}\mathbf{H}_D(i)s^{-i} \quad (45)$$

$$\mathbf{G}^u(s) = \sum_{i=0}^{m}\mathbf{H}_u(i)s^{-i} \quad (46)$$

Equations (45) and (46) can be realized into a system of state space equations using singular value decomposition [31]. In the subsequent analysis, the quantities with hat over them such as $\hat{\mathbf{A}}$, $\hat{\mathbf{B}}$, $\hat{\mathbf{C}}$, $\hat{\mathbf{E}}$, $\hat{\mathbf{L}}_1$, and $\hat{\mathbf{L}}_2$, are constant matrices and they are associated with the realization of the transfer matrices in Eqs. (45) and (46). Let the realization of Eqs. (45) and (46) be symbolically represented by a system of state space equations, i.e.,

$$\dot{\chi}(t) = \hat{\mathbf{A}}\chi(t) + \hat{\mathbf{B}}\mathbf{U}(t) + \hat{\mathbf{E}}\mathbf{D}(t) \quad (47)$$

$$\mathbf{y}(t) = \hat{\mathbf{C}}\chi(t) + \hat{\mathbf{L}}_1\mathbf{U}(t) + \hat{\mathbf{L}}_2\mathbf{D}(t) \quad (48)$$

Equations (47) and (48), combined with the vibratory hub loads expressed in term of disturbance state, Eq. (33), yield the necessary equations for the vibration suppression analysis. Note that the plant, Eq. (47), contains the internal model and the system represented by Eq. (47) is asymptotically stable. Equations (48) can be expressed in term of the solutions to Eq. (47) [32]:

$$\begin{aligned}&\mathbf{y}(t) = \hat{\mathbf{C}}e^{\hat{\mathbf{A}}t}\chi_o + \\ &\hat{\mathbf{C}}\int_0^t e^{\hat{\mathbf{A}}(t-\tau)}\left\{\hat{\mathbf{B}}\mathbf{U}(\tau) + \hat{\mathbf{E}}\mathbf{D}(\tau)\right\}\,d\tau + \\ &\hat{\mathbf{L}}_1\mathbf{U}(t) + \hat{\mathbf{L}}_2\mathbf{D}(t) \\ &= \mathbf{y}_{hom}(t) + \mathbf{y}_u(t) + \mathbf{y}_d(t) + \hat{\mathbf{L}}_1\mathbf{U}(t) + \\ &\hat{\mathbf{L}}_2\mathbf{D}(t) \quad (49)\end{aligned}$$

The vectors $\mathbf{y}_{hom}(t)$, $\mathbf{y}_u(t)$, and $\mathbf{y}_d(t)$ represent the output contributions due to the homogeneous solution, the command, and the disturbance inputs, respectively. Since all the eigenvalues of the plant Eq. (47) are always stable, i.e., $Re\left[\lambda(\hat{\mathbf{A}})\right] < \mathbf{0}$, the condition

$$\lim_{t\to\infty}\mathbf{y}_{hom}(t) = \mathbf{0} \quad (50)$$

is satisfied.

Thus, for steady state disturbance rejection, Eq. (49) must satisfy the following condition:

$$\begin{aligned}&\lim_{t\to\infty}\left\{\mathbf{y}_u(t) + \mathbf{y}_d(t) + \hat{\mathbf{L}}_1\mathbf{U}(t) +\right. \\ &\left.\hat{\mathbf{L}}_2\mathbf{D}(t)\right\} = \mathbf{0} \quad (51)\end{aligned}$$

from which the control vector $\mathbf{U}(t)$, for steady state disturbance suppression, is obtained. Using Eq. (33), the disturbance portion of Eq. (49) can be written as:

$$\mathbf{y}_d(t) = \hat{\mathbf{C}} \int_0^t e^{\hat{\mathbf{A}}(t-\tau)} \hat{\mathbf{E}} \mathbf{C}_d e^{A_d \tau} \chi_{d_o} d\tau \quad (52)$$

Evaluation of Eq. (52), requires the combination of matrices that are function of τ. The combination of the matrix $e^{\mathbf{A}(t-\tau)}$ with the scalar $e^{A_d\tau}$ yields:

$$\mathbf{y}_d(t) = \hat{\mathbf{C}} \int_0^t e^{\hat{\mathbf{A}}t} e^{(j\omega_d \mathbf{I} - \hat{\mathbf{A}})\tau} \hat{\mathbf{E}} \mathbf{C}_d \chi_{d_o} d\tau \quad (53)$$

and by integrating Eq. (53) provides the expression for the rotor disturbance contribution in Eq. (49), i.e.,

$$\begin{aligned} \mathbf{y}_d(t) &= \hat{\mathbf{C}} \left[j\omega_d \mathbf{I} - \hat{\mathbf{A}} \right]^{-1} \hat{\mathbf{E}} \mathbf{D}_o e^{j\omega_d t} - \\ &\quad \hat{\mathbf{C}} e^{\hat{\mathbf{A}} t} \left[j\omega_d \mathbf{I} - \hat{\mathbf{A}} \right]^{-1} \hat{\mathbf{E}} \mathbf{D}_o \end{aligned} \quad (54)$$

where the amplitude vector $\mathbf{D}_o$ represents the force and moment baseline vibrations.

Defining the disturbance transfer matrix, with the internal model incorporated, as a function of the disturbance frequency, $\mathbf{G}_{y_d}(j\omega_d)$:

$$\mathbf{G}_{y_d}(j\omega_d) = \hat{\mathbf{C}} \left[j\omega_d \mathbf{I} - \hat{\mathbf{A}} \right]^{-1} \hat{\mathbf{E}} \quad (55)$$

and substituting equation (55) into equation (54), yields:

$$\begin{aligned} \mathbf{y}_d(t) &= \mathbf{G}_{y_d}(j\omega_d) \mathbf{D}_o e^{j\omega_d t} - \\ &\quad \hat{\mathbf{C}} e^{\hat{\mathbf{A}} t} \left[j\omega_d \mathbf{I} - \hat{\mathbf{A}} \right]^{-1} \hat{\mathbf{E}} \mathbf{D}_o \end{aligned} \quad (56)$$

The second term of equation (56) will decay to zero, since $Re(\lambda(\hat{\mathbf{A}})) < \mathbf{0}$ holds. Hence, the steady state contribution of the disturbance loads in Eq. (49) is given by:

$$\mathbf{y}_{d_s}(t) = \mathbf{G}_{y_d}(j\omega_d) \mathbf{D}_o e^{j\omega_d t} \quad (57)$$

Comparing equations (55) and (49), the steady state contribution of the control vector to the output response is similarly defined as:

$$\mathbf{y}_{u_s}(t) = \mathbf{G}_{y_u}(j\omega_d) \mathbf{U}_o e^{j\omega_d t} \quad (58)$$

with the control transfer matrix defined similar to Eq. (55), i.e.,

$$\mathbf{G}_{y_u}(j\omega_d) = \hat{\mathbf{C}} \left[j\omega_d \mathbf{I} - \hat{\mathbf{A}} \right]^{-1} \hat{\mathbf{B}} \quad (59)$$

The steady state suppression of the disturbances in the frequency domain implies that Eq. (49) must be satisfied, i.e.,

$$\Big\{ \mathbf{G}_{y_u}(j\omega_d) \mathbf{U}_o + \mathbf{G}_{y_d}(j\omega_d) \mathbf{D}_o + \hat{\mathbf{L}}_1 \mathbf{U}_o + \hat{\mathbf{L}}_2 \mathbf{D}_o(t) \Big\} e^{j\omega_d t} = \mathbf{0} \quad (60)$$

The solution to Eq. (60) yields the control amplitudes $\mathbf{U}_o$ required for the disturbance suppression of fuselage vibrations. Since four servo-actuators are used to implement the approach, the four components of the control force vector, $\mathbf{U}_o$ needed for vibration suppression is obtained from the solution of four linear algebraic equations, associated with Eq. (60).

Results and Discussions

The results presented for the coupled rotor/flexible fuselage model are based upon a combination of parameters intended to model approximately an MBB BO-105 helicopter operating at a weight coefficient of C_w=0.005, with a soft-in-plane four bladed hingeless rotor. The results for blade tip responses, vibratory hub loads, fuselage accelerations at various locations of interest, control forces needed to achieve vibration suppression, actuator displacements and power consumption are presented. The sensitivity of the control forces and actuator power requirements to the location where the baseline vibration is measured, are also studied. Table 1 shows that data for a typical soft-in-plane hingeless rotor configuration, for which the calculations are performed, and Table 2 presents the fuselage properties needed for the three dimensional structural dynamic model of the fuselage.

The coupled rotor/flexible fuselage dynamic system and the locations of the servo actuators are shown in Fig. 1, where the heavy dots in the figure identify the non-structural masses located between the corresponding nodes of the beam elements. The servo actuator tip displacements, located at the four corners of the ACSR platform are also shown in Fig. 1. The general implementation of the ACSR system is schematically illustrated in Fig. 2. Figure 3 depicts the unity feedback system and the placement of the internal model for disturbance rejection. In this figure, the internal model is identified as the $\mathbf{D}_I^{-1}(s)$ matrix and the output $\mathbf{y}(s)$ represents the loads transmitted across the servo actuators, i.e., the disturbances and forces in the springs which are installed parallel to the actuators.

Figures 4 and 5 depict the hub loads as a function of advance ratio, for the case when the actuators are disengaged and engaged. Figure 4 shows that when the actuators are engaged, the hub forces are not substantially higher than those corresponding to the baseline (or uncontrolled) values. Figure 5 shows that the hub moments for the controlled and baseline values are also quite similar regardless of actuators activity. Figures 6 through 8 illustrate the fuselage accelerations at various fuselage locations corresponding to the rear cabin, pilot seat, the actuator tips (upper front actuators), and the helicopter center of gravity, as a function of the advance ratio. Figure 6 shows that when the controller, based on the IMP approach, is engaged, the fuselage accelerations in the longitudinal direction, for all locations considered, are reduced to levels below 0.02g. Figures 7 and 8 indicate that similar observations can be made for the fuselage accelerations in the lateral and vertical directions, when the controller is engaged. It is evident from Figs. 6-8 that the highest levels of baseline acceleration are encountered in the vertical and lateral direction. It is particularly interesting to note that uncontrolled vibrations in the vertical direction are between 0.2-0.38g at the high advance ratio of $\mu = 0.40$. Recall that stall and compressibility have been neglected, therefore these high vibration levels are probably not reliable estimates. However, it is remarkable that despite these high levels of baseline vibration the controller encounters no difficulty in reducing these vibrations below acceptable levels.

Figure 9 depicts the nondimensional blade tip deflections as a function of blade azimuth, for the case when the actuators are engaged and disengaged, at an advance ratio of $\mu = 0.3$. In this figure, both control approaches are shown: the basic disturbance rejection scheme (ACSR) which was formulated without using an internal model [16], as well as the case based on using the IMP approach. This figure clearly indicates that when the controller is active, the rotor blade tip flap, lag, and torsional deflections, remain virtually unchanged and thus vehicle airworthiness is unaffected.

In our earlier research [16], a simple control scheme denoted by the label ACSR was considered and fairly high control forces were required for vibration reduction. Figure 10 presents a comparison of the control forces required in the actuators as a function of the advance ratio when the earlier (ACSR) approach and the current (IMP) approach are implemented. From Fig. 10, it is evident that the actuators need substantially smaller forces to achieve similar vibration reduction, if the controller is based on the IMP approach instead of the basic disturbance rejection scheme (ACSR), described in Ref. 16. Figure 11 shows the actuator tip displacements as a function of advance ratio, for the case when the actuators are disengaged and engaged. The information shown in Fig. 8, 10 and 11 indicates that while the actuators requires considerable forces for vibration suppression, the actuators tip displacements are relatively small. Note that the indices 2 and 3 in Fig. 11 denote the upper front actuators' tip locations.

Figure 12 depicts the actuators power consumption as a function of advance ratio. The actuator power consumption is calculated from the product of the actuator force and its rate of net displacement - $Pw_i = F_i * N_b\Omega * W_i$ where Pw_i denotes the power consumption of the i^{th} actuator, F_i represents the force generated by the i^{th} actuator, and W_i denotes the net displacement of the i^{th} actuator. The total power consumption is obtained by summing over the four actuators. The expression derived here for the power represents the maximum power required. The effectiveness of the proposed control approach is apparent in this figure; the actuators need small amount of power to achieve substantial vibration reduction in the fuselage.

The sensitivity of the actuator control force and power consumption as a function of the locations of the baseline vibration measurements is illustrated in Figs. 13 and 14, respectively. Figure 13 presents two families of control force curves as a function of the advance ratio. The family labeled station 1, corresponds to the mid-cabin location where the vertical displacement is large, and station 2 corresponds to the rear cabin location. For our case, the relative difference between the vertical displacements in these two locations are among the larger ones. It should be emphasized that the control forces shown in Fig. 13 are based upon the baseline vibration levels employed by the IMP algorithm. These correspond the the mid-cabin and rear cabin locations, as shown in Fig. 1. Figure 13 indicates that although the control forces in the actuators are sensitive to the locations of baseline vibration measurements, this sensitivity is relatively mild. Based on the results shown in Fig. 14, it is evident that a similar observation can be made for the sensitivity of the actuator power requirement.

Concluding Remarks

A refined coupled rotor/flexible fuselage aeroelastic response model for vibration suppression study is formulated. The fuselage contains a provision for the modeling a novel type of vibration suppression device, denoted by the term ACSR. Furthermore, the fuselage is represented by a fairly elaborate finite element model, which accounts for the effect of important non-structural masses.

The coupling between the rotor and the fuselage is accomplished implicitly by satisfying force and moment equilibrium at the hub. The approach combines a nonlinear rotor model, where the nonlinearities are due to moderate blade deflections, with a flexible fuselage represented by a linear finite element model.

A controller based on IMP is implemented in conjunction with a coupled rotor/flexible fuselage model. Numerical results indicate that the controller based on IMP can reduce vibration levels, below 0.05g, for all fuselage locations considered. In addition, the proposed controller does not influence the vehicle airworthiness; this is to be expected since the actuators are implemented in the non-rotating system.

The numerical simulations reveal that the control forces for vibrations reduction required by the actuators depend on the control algorithm employed. The simpler control algorithm denoted as the ACSR algorithm, needs substantially larger forces than the control algorithm based on the IMP, to achieve a similar level of vibrations reduction. The study shows that fairly large control forces are needed for vibration reduction, however these are accompanied by small actuator displacement. The overal power consumption needed for vibration suppression is small.

The sensitivity of the control forces in the actuators and the associated actuator power consumption depends on the locations where the baseline vibrations are measured; however, this dependency is mild.

Aknowledgement

This research was supported by the U.S. Army Research Office under grant No. DAA H04-93-G-0004, with Dr. Gary Anderson as technical monitor.

References

[1] Crews, S.T.,"Rotorcraft Vibration Criteria: A New Perspective," Proceedings of the 43rd Annual Forum of the American Helicopter Society, St. Louis, Missouri, May 1987.

[2] Aeronautical Design Standard (ADS-27),"Requirements for Rotorcraft Vibration Specifications, Modeling and Testing," U.S. Army Aviation System Command, Novermber 1986.

[3] Reichert, G.,"Helicopter Vibration Control - A Survey," *Vertica*, Vol. 5, No. 1, 1981.

[4] Loewy, R.G.,"Helicopter Vibrations: A Technological Perspective," *Journal of the American Helicopter Society*, Vol. 29, No. 4, October 1984, pp. 4-30.

[5] Kvaternik, R.G., Bartlett, F.D., Jr., and Cline, J.H.,"A Summary of Recent NASA/ARMY Contributions to Rotorcraft Vibrations and Structural Dynamics Technology," NASA/ARMY Rotorcraft Technology, NASA-CP 2495, 1988.

[6] Friedmann, P. P., "Helicopter Vibration Reduction Using Structural Optimization with Aeroelastic/Multidisciplinary Constraints-A Survey," *Journal of Aircraft*, Vol. 28, No. 1, 1991, pp. 8-21.

[7] Friedmann, P. P., and Millot, T.A. "Vibration Reduction in Rotorcraft Using Active Control: A Comparison of Various Approaches," *Journal of Guidance, Control, and Dynamics*, Vol. 18, No. 4, July-August 1995.

[8] King, S.P., and Staple, A.E., "Minimization of Helicopter Vibraton Through Active Control of Structural Response," *Rotorcraft Design Operations*, AGARD-CP-423, October 1986, pp. I4-1-I4-13.

[9] Y. Niwa and N. Katayama, "Active Vibraton Reduction System for a Helicopter," 20^{th} European Rotorcraft Forum, Amsterdam, Netherland, Oct. 1994, pp. 70-01 70-14.

[10] H. Kawaguchi, S. Bandoh, and Y. Niwa, "The Test Results for AVR (Active Vibration Reduction) System," Presented a the American Helicopter Society 52^{nd} Annual Forum, Washington, D.C., June 4-6, 1996, pp. 123-136.

[11] Staple, A.E.,"An Evaluation of Active Control of Structural Response as a Means of Reducing Helicopter Vibration," *Proceedings of the 15th European Rotorcraft Forum*, Amsterdam, Netherlands, September 1989, pp. 3-17.

[12] Welsh, W.A., Von Hardenberg, P.C., Von Hardenberg, P.W., and Staple, A.E.,"Test and Evaluation of Fuselage Vibration Utilizing Active Control of Structural Response(ACSR) Optimized to ADS-27," *Proceedings of 46th Annual Forum of the American Helicopter Society*, Washington, DC May 1990, pp. 21-37.

[13] Welsh, W. et al, "Flight Test on an Active vibration Control System on the UH60 Black Hawk Helicopter," *Proceedings of the* 51^{th} *Annual Forum of the American Helicopter Society*, Fort Worth, TX, May 9-11, 1995, pp. 393-402.

[14] Chiu, T. and Friedmann, P. P., "A Coupled Helicopter Rotor/Fuselage Aeroelastic Response Model for ACSR," AIAA-95-1226-CP, *Proceedings of 36th AIAA/ASME/ASCE/AHS/ASC Structures, Structural Dynamics and Materials Conference*, New Orleans, LA, April 10-13, pp. 574-600, 1995.

[15] Chiu, T. and Friedmann, P. P., "ACSR System for Vibration Suppression in Coupled Helicopter Rotor/Flexible Fuselage Model," AIAA-96-1547-CP, *Proceedings of* 37^{th} *AIAA/ASME/ASCE/AHS/ASC Structures, Structural Dynamics and Materials Conference*, Salt Lake City, UT, April 14-17, pp. 1972-1991, 1996.

[16] Chiu, T. and Friedmann, P. P., "Vibration Suppression in Helicopter Rotor/Flexible Fuselage System Using the Active Control of Structural Response (ACSR) Approach with Disturbance Rejection," Presented at the American Helicopter Society 52^{nd} Annual Forum, Washington, D.C., June 4-6, pp. 736-757, 1996.

[17] Venkatesan C., and Friedmann, P. P., "Aeroelastic Effects in Multi-Rotor Vehicles with Applications to a Heavy-Lift System, Part 1 : Formulation of Equations of Motion," NASA-CR 3822, August 1984.

[18] Venkatesan C., and Friedmann, P. P., "Aeroelastic Effects in Multi-Rotor Vehicles, Part 2: Method of Solution and Results Illustrating Coupled Rotor-Fuselage Aeromechanical Stability," NASA-CR 4009, 1986.

[19] Papavassiliou, I., Friedmann, P. P. and Venkatesan, C., "Coupled Rotor/Fuselage Vibration Reduction Using Open-Loop Blade Pitch Control," Mathematical Computer Modeling, Vol. 18, No. 3/4, pp. 131-156, 1993.

[20] Vellaichamy, S. and Chopra, I., "Aeroelastic Response of Helicopters with Flexible Fuselage Modeling," AIAA Paper 92-2567-CP, *Proceedings of 33rd AIAA/ASME/ ASCE/AHS/ASC 33rd Structures, Structural Dynamics and Materials Conference*, Dallas, TX, April 13-15, pp. 2015-2026, 1992.

[21] Vellaichamy, S. and Chopra, I., "Effect of Modeling Techniques in the Coupled Rotor-Body Vibraton Analysis," AIAA 93-1360-CP, *Proceedings of 34th AIAA/ASME/ ASCE/AHS/ASC Structures, Structural Dynamics and Materials Conference*, La Jolla, CA, April 19-22, pp. 53-575, 1993.

[22] Rosen, A., and Friedmann, P.P., "Nonlinear Equations of Equilibrium for Elastic Helicopter or Wind Turbine Blades Undergoing Moderate Deformation," NASA CR-159478, December 1978.

[23] ___, "MACSYMA: Reference Manual," Symbolics Inc., June 1986.

[24] Greenberg, J.M.,"Airfoil in Sinusoidal Motion in a Pulsating Stream," NACA-TN 1326, 1947.

[25] Shamie, J., and Friedmann, P. P.,"Effect of Moderate Deflections on the Aeroelastic Stability of a Rotor Blade in Forward Flight," Paper No. 24, Proceedings of the 3rd European Rotorcraft and Powered Lift Aircraft Forum, Aix-en-Provence, France, September 1977.

[26] Surana, K.,"Consistent Mass Matrices for Three Dimensional Beam Element Due to Distributed and Lumped Non-Structural Mass Systems Acting on its Span," *Computers and Structures*, Vol. 13, pp. 515-524, 1981.

[27] Stoppel, J. and Degener,"Investigations of Helicopter Structural Dynamics and a Comparison with Ground Vibration Tests," AHS Journal, Vol. 27, April 1982, pp. 34-42.

[28] Stephens, W.B. and Peters, D.A.,"Rotor-Body Coupling Revisited," AHS Journal, Vol. 32, No. 1, Jan 1987, pp. 68-72.

[29] ___,"IMSL Library: Reference Manual," IMSL Inc., Houston, Texas, 1980.

[30] Petry, J., "Servo-Actuator Control for Sampled-Data Feedback Disturbance Rejection," *European Space Agency*, Translation of DFVLR-FB-86-08, Nov. 1987.

[31] Chen, C.T., *Linear System Theory and Design*, CBS College Publishing, 1984.

[32] Rosenbrock, H.H., *State-Space and Multivariable Theory*, London: Nelson and Sons Ltd, 1979.

Table 1: Blade data for rotor configuration

$C_W = 0.005$;	$c/R = 0.055$
$\sigma = 0.07$;	$\beta_p = 0.0$
$h_1/R = 0.2851$;	$h_2/R = 0.2851$
$a = 2\pi$;	$fC_{d_f}/\pi R^2 = 0.01$
Soft-in-plane four bladed rotor	
stiffnesses & frequencies	
$EI_y/m_b\Omega^2 R^2 = 0.0106$	
$EI_z/m_b\Omega^2 R^2 = 0.0301$	
$GJ/m_b\Omega^2 R^2 = 0.001473$	
$\omega_{F_1} = 1.124$;	$\omega_{F_2} = 3.407$
$\omega_{F_3} = 7.617$	
$\omega_{L_1} = 0.7311$;	$\omega_{L_2} = 4.453$
$\omega_{T_1} = 3.175$;	$\omega_{T_2} = 9.097$
All blade offsets are zero.	

Table 2: Data for the three dimensional structural dynamic model of the fuselage

$A/L_b^2 = 0.788x10^{-4}$;	$E/m_b\Omega^2 = 0.662x10^7$
$G/m_b\Omega^2 = 0.249x10^7$;	$\rho/m_b/R^2 = 0.119x10^5$
$I_x/R^4 = 0.193x10^{-8}$;	$I_y/R^4 = 0.966x10^{-9}$
$I_z/R^4 = 0.966x10^{-8}$;	$I_p/R^4 = 0.966x10^{-9}$
$elements = 300$	
$d.o.f's = 966$	
$nodes = 161$	

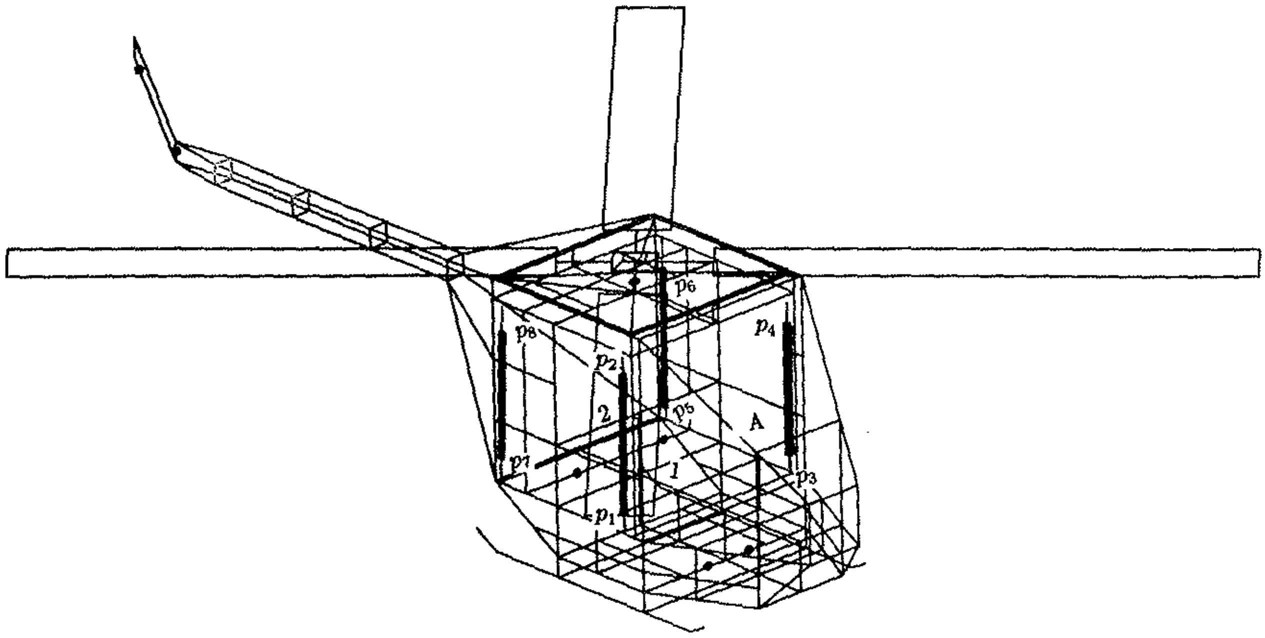

Figure 1: Coupled rotor/active control/fuselage dynamic system

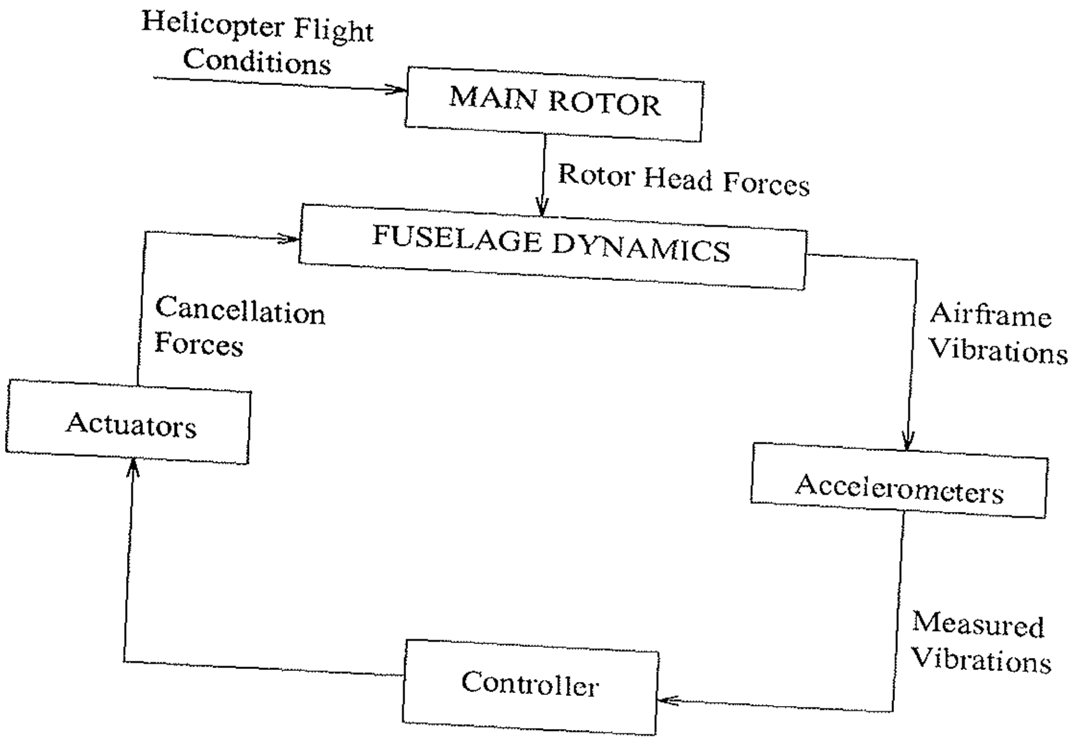

Figure 2: Helicopter System Schematic for ACSR

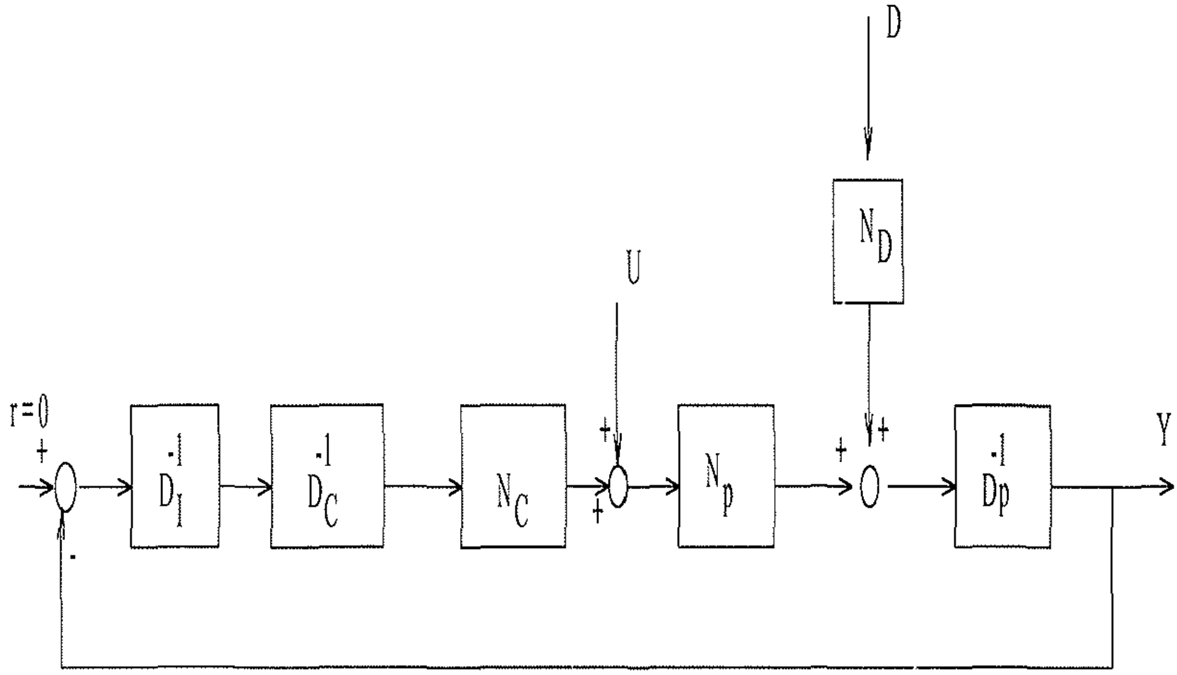

Figure 3: Placement of internal model for disturbance rejection

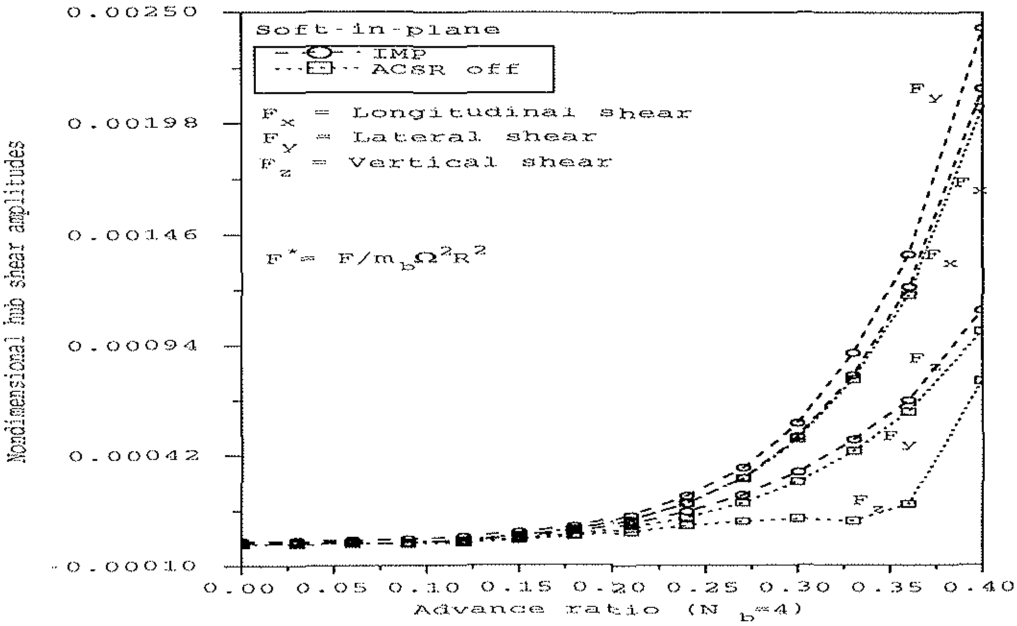

Figure 4: Hub shears vs. advance ratio, baseline(uncontrolled) and with IMP control

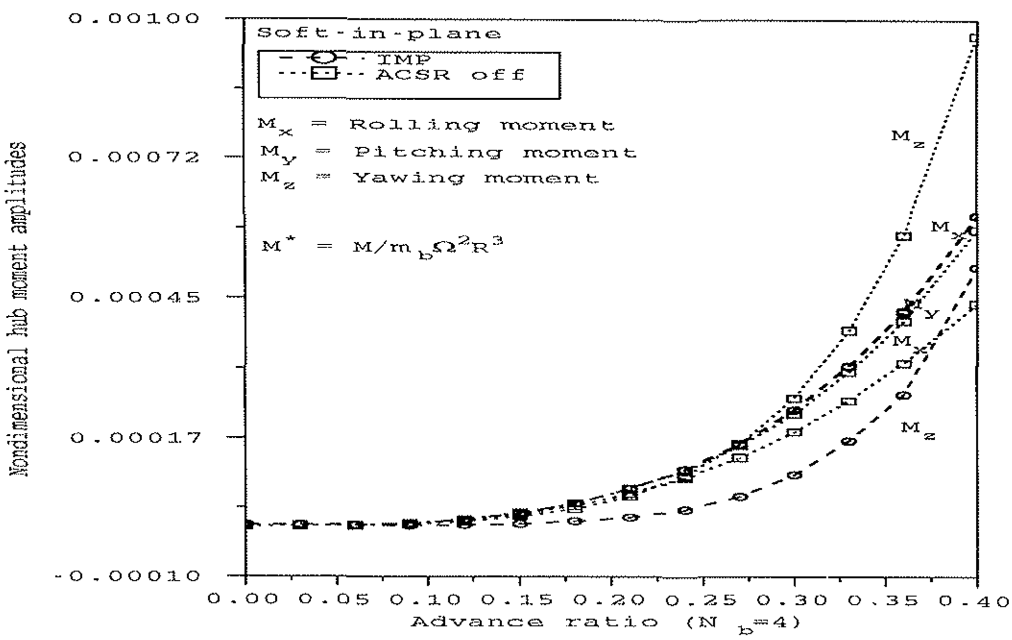

Figure 5: Hub moments vs. advance ratio, baseline(uncontrolled) and with IMP control

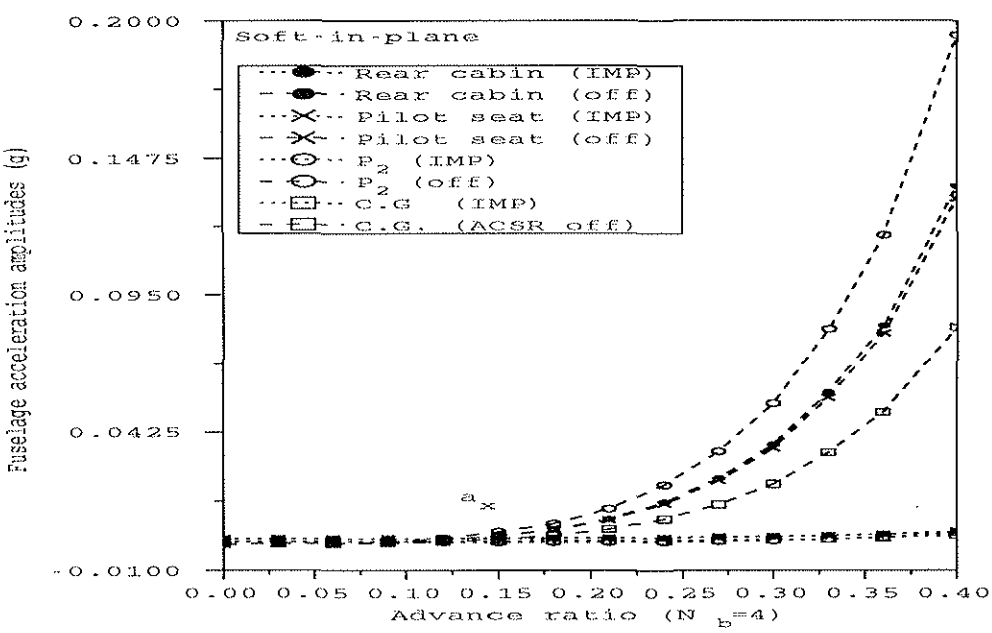

Figure 6: Fuselage accelerations vs. advance ratio, longitudinal(x) direction, with controller engaged or disengaged

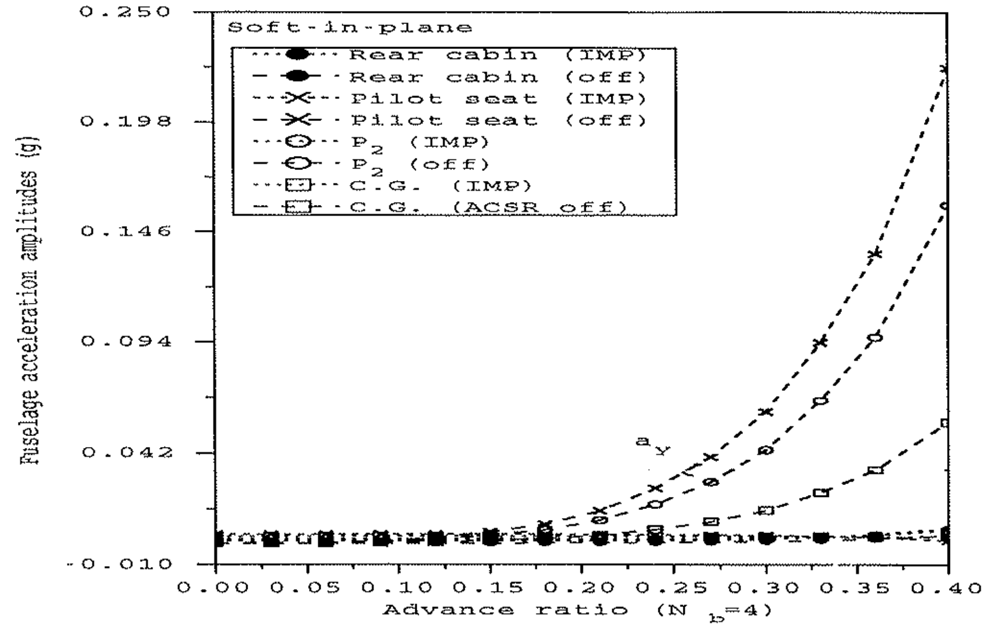

Figure 7: Fuselage accelerations vs. advance ratio, lateral(y) direction, with controller engaged or disengaged

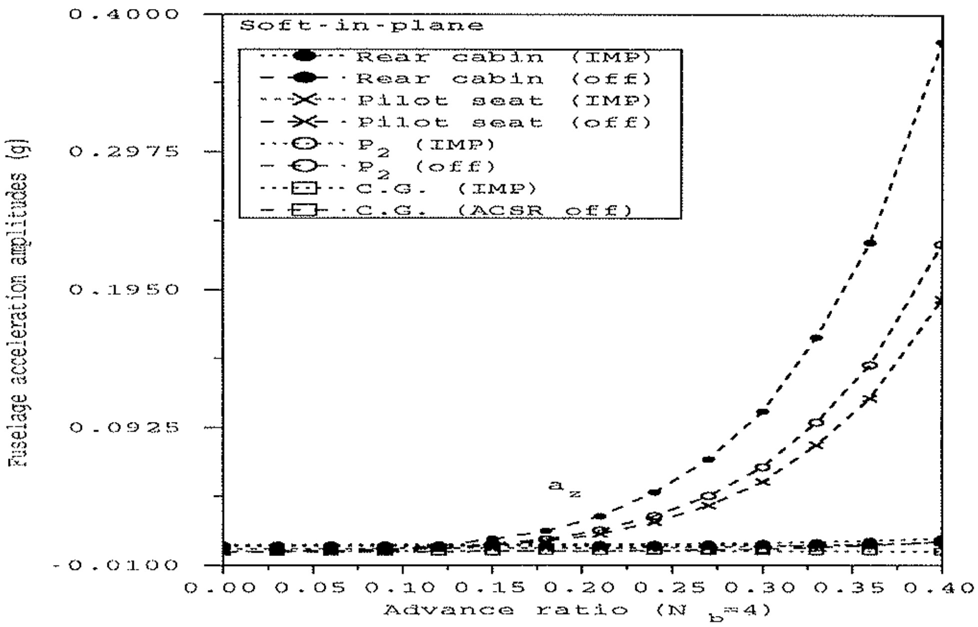

Figure 8: Fuselage accelerations vs. advance ratio, vertical(z) direction, with controller engaged or disengaged

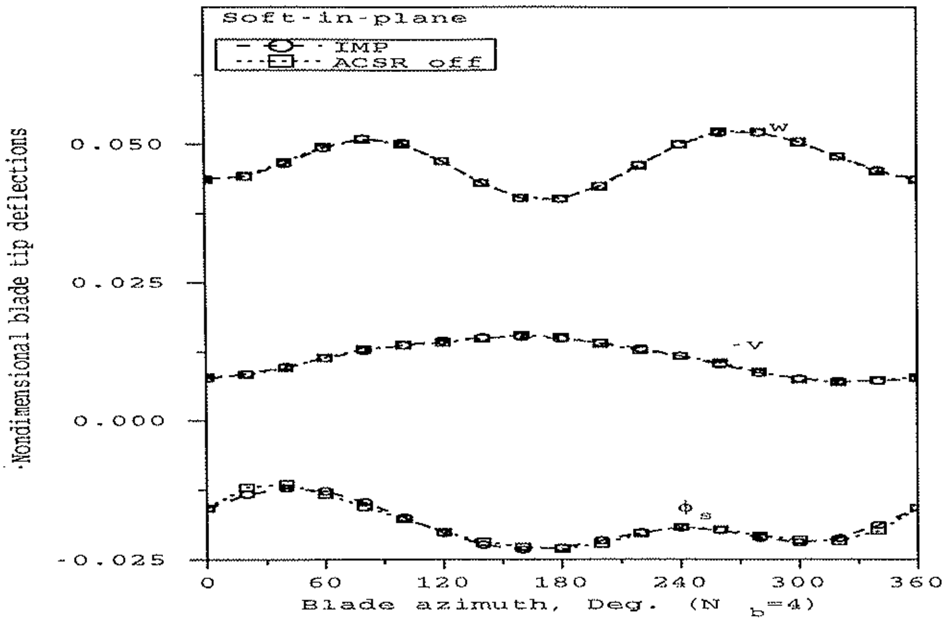

Figure 9: Blade tip deflections, with controller engaged or disengaged at μ =0.3

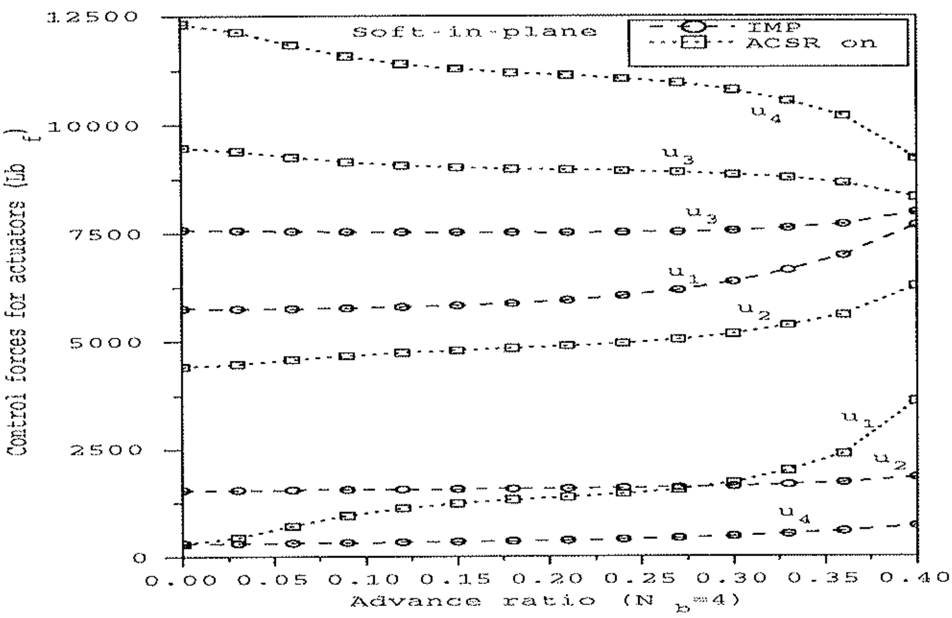

Figure 10: Actuators control forces (lb_f), comparison of the two control approaches

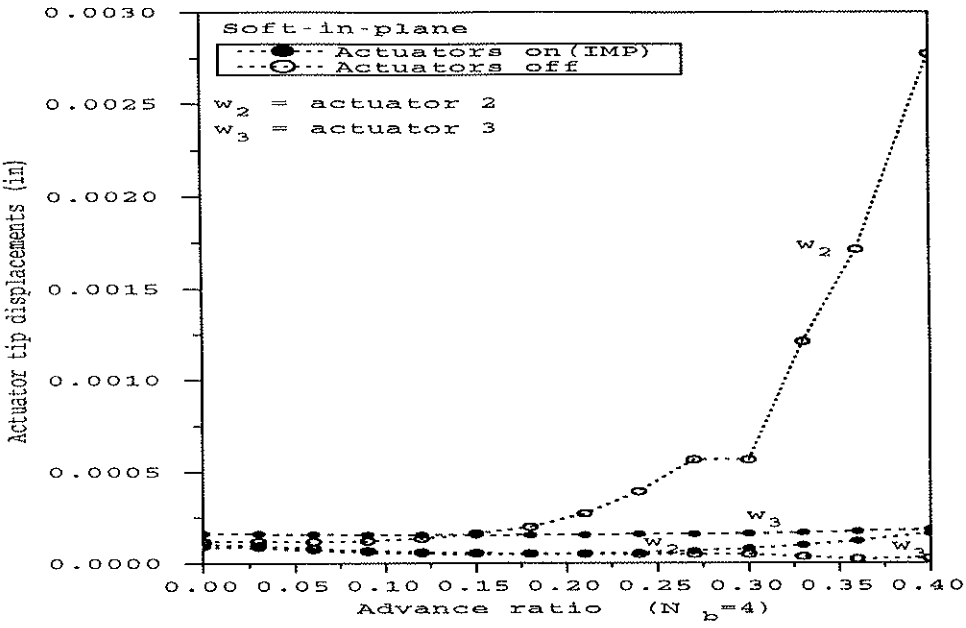

Figure 11: Actuators tip displacements vs. advance ratio with controller engaged or disengaged

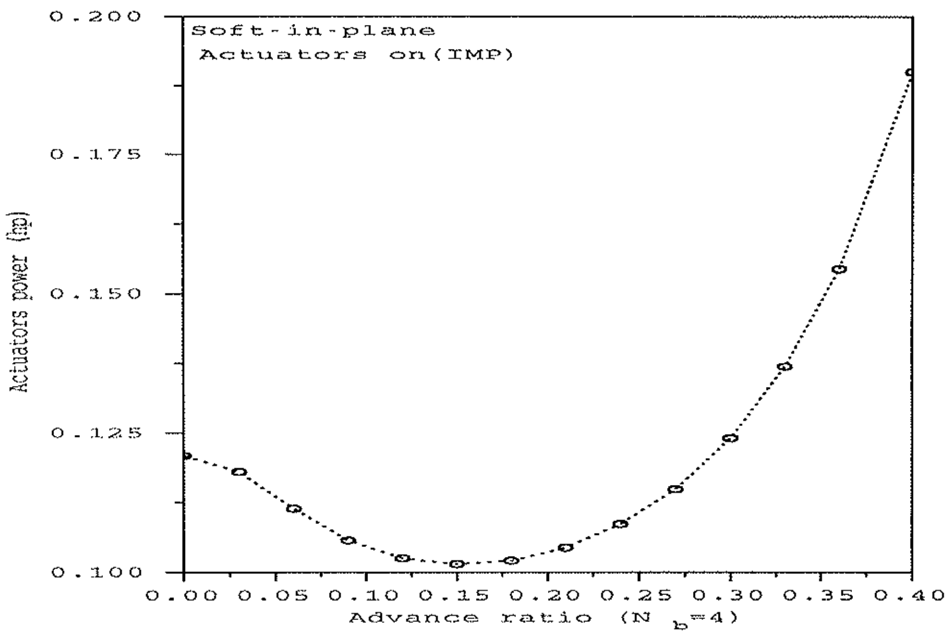

Figure 12: Actuators power requirement for IMP

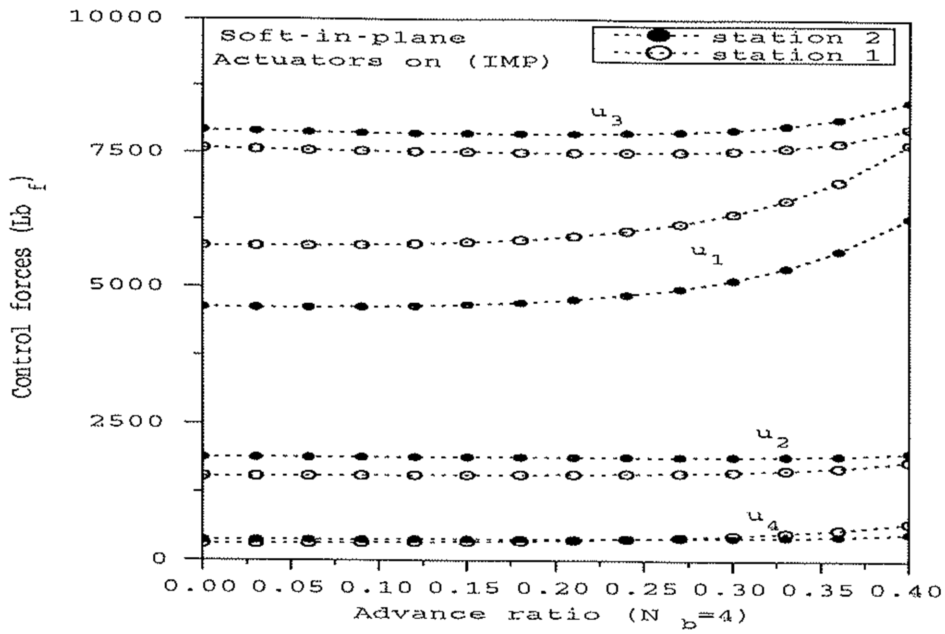

Figure 13: Control forces vs. advance ratio, with controller engaged

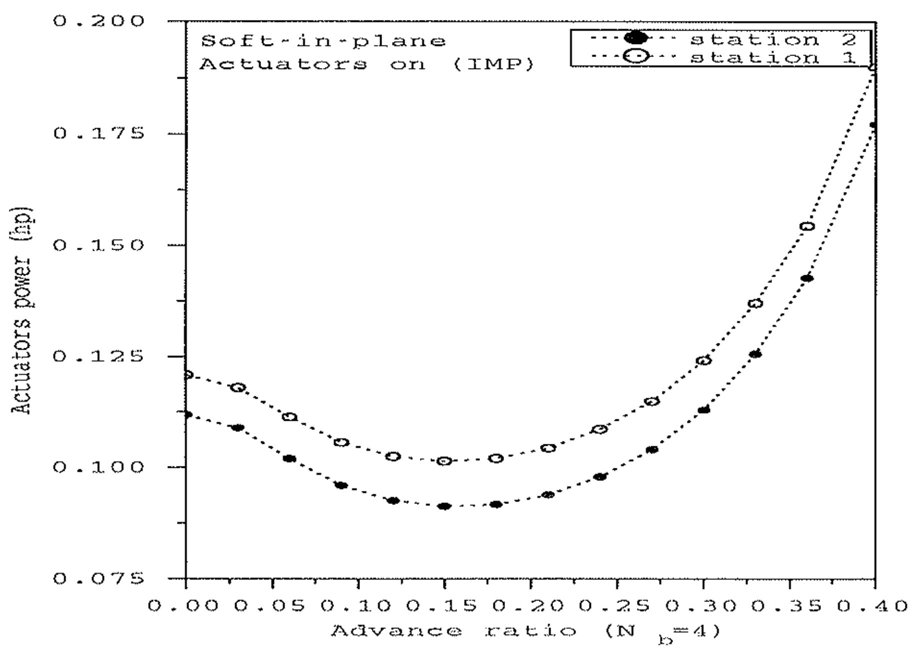

Figure 14: Actuators power requirement sensitivity to location of vibration(baseline) measurement